Journal of Solid State Chemistry **157,** 149–159 (2001)
doi:10.1006/jssc.2000.9067, available online at http://www.idealibrary.com on IDEAL®

Synthesis of Nanosize Yttria-Stabilized Zirconia by a Molecular Decomposition Process

Yi Jiang, Sanjeevani V. Bhide, and Anil V. Virkar[1]

Department of Materials Science and Engineering, 122 South Central Campus Drive, Room 304, University of Utah, Salt Lake City, Utah 84112

Received July 12, 2000; in revised form December 4, 2000; accepted December 8, 2000

Nanosize yttria-stabilized zirconia (YSZ) was synthesized by a novel approach based on molecular decomposition. In this approach, yttria-doped $BaZrO_3$ (Y–$BaZrO_3$) or yttria-doped Na_2ZrO_3 (Y–Na_2ZrO_3) precursors were first synthesized from $BaCO_3$, ZrO_2, and Y_2O_3 or $BaCO_3$ and commercial YSZ for Y–$BaZrO_3$, and from Na_2CO_3 and YSZ for Y–Na_2ZrO_3, by a conventional solid-state reaction method. The precursors were then boiled to leach away the unwanted species, BaO or Na_2O, either in a dilute HNO_3 solution in water in the case of Y–$BaZrO_3$, or in deionized water in the case of Y–Na_2ZrO_3. During boiling in HNO_3 or water, the residue of Zr–Y–O skeleton formed fine, nanosize YSZ particles. The particle size of the as-synthesized nanosize powders estimated from X-ray diffraction peak broadening was ~2–3 nm, while that estimated from specific surface area measurements by BET adsorption isotherm was ~15 nm. Examination under a transmission electron microscope showed that the crystallite size was ~5 nm. Samples were also examined by Raman spectroscopy to determine the crystallographic polymorph of the YSZ formed. Subsequent heating in air led to particle growth. However, even when the particles were heated to a temperature as high as 1000°C, the particle size was well in the nanosize range. © 2001 Academic Press

Key Words: **nanosize powder; yttria-stabilized zirconia (YSZ); molecular decomposition.**

I. INTRODUCTION

Nanosize powders have numerous applications as, e.g., catalysts, photocatalysts, electrocatalysts, catalyst supports (1), electrodes, active powders for the fabrication of dense bodies (2), semiconductors for energy storage, photovoltaics (3), ultrafine magnetic materials for information storage (4), destructive adsorbents in environmental cleanup (5), in water purification (6), and in optical computers (7), to name a few. The synthesis of nanosize materials has received considerable attention over the past decade or so. Several processes have been developed and are currently being used for the synthesis of nanosize powders. These processes include gas-phase condensation, mechanical milling (8), thermal crystallization, chemical precipitation (9), sol–gel process, and aerosol spray pyrolysis (10).

In gas-phase condensation, evaporation of precursors and their interaction with an inert gas leads to loss of kinetic energy, and homogeneous nucleation of nanosize powders occurs in a supersaturated vapor (11). Nanocrystalline powders of TiO_2 (12), Li_2O-doped MgO (13), CeO_2 (14), Y-doped ZrO_2 (15), etc. have been produced by gas-phase condensation. Aerosol spray pyrolysis has been used to synthesize $BaFe_{12}O_{19}$ (16) and Fe_2O_3 (17) among other materials. High-energy mechanical milling is used extensively to produce nanomaterials, especially when large quantities of materials are required. Very fine particles of nickel–aluminum alloys (18), Fe–Co–Ni–Si alloys (19), and Ni–Mo alloys (20), for example, have been produced by mechanical milling. Contamination by the milling process, however, is a shortcoming of this process. Also, although very fine particles can be made, agglomeration is a problem leading to cluster sizes in the micron range.

Chemical coprecipitation has been studied extensively for the synthesis of nanosize powders (9). Metallic as well as ceramic powders can be made by carefully controlling the chemistry. Alkali metal borohydride, MBH_4, where M is an alkali metal, for example, has been used as a reducing agent in aqueous media for the synthesis of metallic powders. It is important to control the pH and the ionic strength in aqueous media to prevent Ostwald ripening (9). In the synthesis of nanosize iron oxide, for example, it has been shown that the higher the pH and the higher the ionic strength, the smaller is the size of nanosize particles.

In this communication, we report a novel approach developed for the synthesis of nanosize yttria-stabilized zirconia (YSZ) powder. There are many reports in the literature on the synthesis of nanosize YSZ powders by processes such as sol–gel process (21), inert gas condensation (22), plasma technique (23), chemical coprecipitation (24), and aerosol combustion (25). All of these methods are based on molecular synthesis of nanoparticles wherein the particles are built-up by an atom-by-atom or by a molecule-by-molecule

[1] To whom correspondence should be addressed.

0022-4596/01 $35.00

addition. Thus, the growth of particles inevitably occurs during the process itself. In order to ensure the formation of nanosize powders, in such processes, a careful control over nucleation and growth is required.

The approach we report in this paper is based on molecular decomposition, rather than molecular synthesis, in which a precursor powder (either of a micro or macro size, containing the desired elements) is first synthesized by a conventional method, such as a high-temperature solid-state reaction. The unwanted species are then chemically leached away in a suitable liquid, which may be just water, or a dilute acid solution (26). During the leaching process, the concomitant change in volume and crystal evolution leads to the formation of very fine (molecular level) fragments, thus leading to the formation of nanosize powders. Since neither the precursor nor the product is soluble in the selected liquid, growth of particles, which necessarily requires the occurrence of dissolution–reprecipitation, cannot occur. Therefore, particle coarsening can be successfully prevented. This approach may be also ideally suited for the commercial production of nanosize powders since the process requires neither exotic equipment nor exotic chemistry. In the present communication, 8 mol.% yttria-stabilized zirconia (YSZ) nanosize powder was successfully prepared by this approach using two different precursors, 8 mol.% yttria-doped Na_2ZrO_3 (Y–Na_2ZrO_3) and 8 mol.% yttria-doped $BaZrO_3$ (Y–$BaZrO_3$). In the case of Y–Na_2ZrO_3, the liquid used was water. In the case of Y–$BaZrO_3$, the liquid used was dilute nitric acid. The powders synthesized using either precursor were nanosize, as determined by X-ray diffraction (XRD) and specific surface area measurement. Transmission electron microscopy (TEM) confirmed the nanosize of the crystallites formed. Also, it was determined by XRD that the as-synthesized powders are either cubic or tetragonal, but not monoclinic. Raman spectroscopy confirmed the formation of the cubic structure.

II. EXPERIMENTAL PROCEDURE

For the synthesis of nanosize yttria-stabilized zirconia by the present method, the precursor can be a suitable alkali or an alkaline earth zirconate. Two types of precursors, namely, yttria-doped barium zirconate (Y–$BaZrO_3$) and yttria-doped sodium zirconate (Y–Na_2ZrO_3), were synthesized by a conventional solid-state reaction method. For preparing Y–$BaZrO_3$, the starting materials, namely, $BaCO_3$, ZrO_2, and Y_2O_3, or $BaCO_3$ and a commercial yttria-stabilized zirconia (YSZ) powder, were mixed in the requisite proportions, wet ball-milled, in alcohol for 24 h and then dried. For the synthesis of Y–Na_2ZrO_3, Na_2CO_3 and commercial YSZ powder were mixed in the requisite proportion, wet ball-milled, and then dried. The ball-milled and dried powder mixtures were calcined at various temperatures and the resulting powders were examined by XRD with Cu$K\alpha$ radiation to identify calcination conditions which ensured the formation of completely converted, single-phase, precursor powders, i.e., Y–$BaZrO_3$ or Y–Na_2ZrO_3.

Doped sodium zirconate was then boiled and washed in deionized water since the reaction between Na_2ZrO_3 and water is thermodynamically favored. In this way, Na_2O can be easily leached out. To ensure the complete removal of Na_2O, the powder was continuously washed until the pH of the solution was nearly neutral ($\sim$7). The resulting powder was then dried and later characterized. The Gibbs free energy change for the reaction of barium zirconate with water at or near room temperature is close to zero (27), indicating that $BaZrO_3$ is thermodynamically stable in the presence of water. Thus, water is not a suitable leaching agent for $BaZrO_3$. A dilute acid solution is necessary to facilitate the removal of BaO from barium zirconate. Y-doped barium zirconate was boiled in dilute HNO_3 acid (0.07 M) repeatedly until no further change in pH of the solution occurred. The powder was then thoroughly washed with deionized water and dried. In both cases, the leaching solution as well as the as-synthesized powder were chemically analyzed using the inductively coupled plasma (ICP) technique. For the analysis of the as-synthesized YSZ powder by ICP, samples were dissolved in concentrated HCl. The as-synthesized powders were also examined by XRD with Cu$K\alpha$ radiation. The objective was to determine the crystal structure and to estimate the particle size by line broadening. Specific surface area was measured by Brunauer–Emmett–Teller (BET) adsorption isotherm using nitrogen gas.

Raman spectra were obtained to determine the crystallographic polymorph of the YSZ formed with an Ar plasma laser (Spectra-Physics, Model 2580) and a 0.6-m triple spectrometer (Spex Industries, Inc., Model 1877). The spectrometer was calibrated using Ar laser plasma lines. A 488-nm laser was focused on the sample with a beam diameter of 1 mm. The plasma lines were removed from the laser beam using a 10-nm bandpass filter. The spectrometer slit width was adjusted to 20 nm.

One of the samples was also examined under a transmission electron microscope (TEM) to estimate the crystallite size of as-synthesized YSZ using a JEOL 4000FX transmission electron microscope.

Differential thermal analysis (DTA) was conducted on the as-synthesized YSZ powders. In the DTA experiments, the samples were purged with purified air and heated to 1200°C at a heating rate of 10°C/min. Based on the DTA information, several temperatures were identified for the calcination of the powders after the leaching treatments. The as-synthesized YSZ powders were subsequently calcined at various temperatures up to a maximum of 1000°C. The calcined powders were further examined by XRD.

III. RESULTS AND DISCUSSION

Figures 1a and 1b show XRD patterns of Y–$BaZrO_3$ powders made by calcining mixtures of $BaCO_3$, ZrO_2, and Y_2O_3, and mixtures of $BaCO_3$ and YSZ, respectively, at 1250°C for 2 h. The patterns are almost identical and match the standard pattern for the cubic structure of perovskite, $BaZrO_3$. Figure 1b shows the presence of a single-phase perovskite structure. In Fig. 1a, small peaks, indicating the existence of a small amount of a second phase, can be seen. Overlap of peaks prohibits an unequivocal determination of the second phase. However, the peak positions of the second phase are consistent with cubic or tetragonal zirconia. Presumably, the precursor was not fully homogenized under the chosen calcination conditions. The results nevertheless show that yttria-doped $BaZrO_3$ can be synthesized with either of the starting materials at a temperature of 1250°C or above. Figure 2 is an XRD pattern of a mixture of Na_2CO_3 and YSZ after calcining at 1250°C for 2 h, which corresponds to monoclinic sodium zirconate, Na_2ZrO_3. Since YSZ was used instead of ZrO_2, it is expected that the Na_2ZrO_3 formed should be yttria-doped, i.e., Y–Na_2ZrO_3. Again, XRD revealed that the reaction was complete and resulted in the formation of a single phase, within the accuracy of the XRD technique. A calcination temperature lower than 1050°C was not high enough to ensure the completion of the reaction, as evidenced by the lack of formation of a single-phase material.

TABLE 1
Chemical Analysis of the Leaching Solution (Dilute HNO_3) after Boiling Y–$BaZrO_3$ in It

Powder	Solution	Barium (mol/l)	Yttrium (mol/l)	Zirconium (mol/l)
Y–$BaZrO_3$	0.3 M HNO_3	0.104	7.11×10^{-4}	$< 2.0 \times 10^{-5}$
Y–$BaZrO_3$	0.07 M HNO_3	0.062	3.0×10^{-5}	$< 2.0 \times 10^{-5}$

Chemical leaching of BaO from yttria-doped $BaZrO_3$ (Y–$BaZrO_3$) precursor was achieved in a dilute HNO_3 solution in water. The precursor was boiled in a dilute HNO_3 acid solution, filtered, and washed repeatedly until the solution pH was unchanged. It was then thoroughly washed using deionized water to completely remove Ba as $Ba(NO_3)_2$. The solution containing leachable ions was chemically analyzed to determine the concentrations of Ba, Y, and Zr. The results showed (Table 1) a significant concentration of Ba^{2+} but only trace concentrations of Zr^{4+} and Y^{3+}, confirming that Ba^{2+} was selectively dissolved and led to the formation Y_2O_3–ZrO_2, which is essentially insoluble in dilute HNO_3, by a reaction such as

$$Y\text{–}BaZrO_3 + 2HNO_3 \rightarrow Ba(NO_3)_2 + Y_2O_3\text{–}ZrO_2 + H_2O. \quad [1]$$

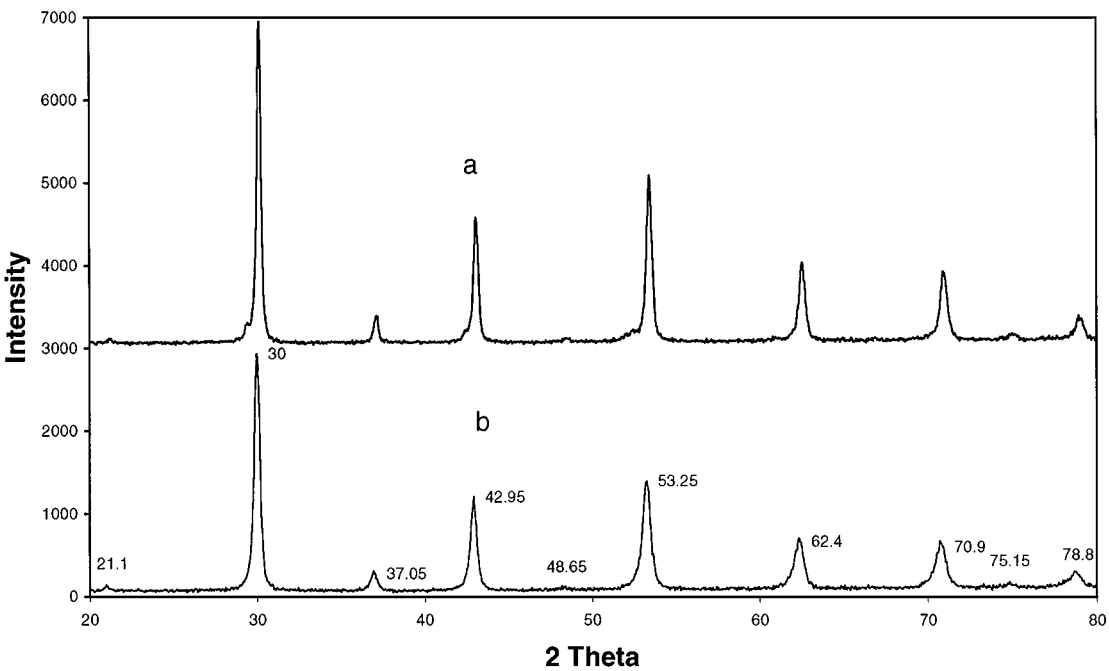

FIG. 1. (a) XRD pattern of yttria-doped $BaZrO_3$ powder synthesized by calcining a mixture of $BaCO_3$, ZrO_2, and Y_2O_3 at 1250°C for 2 h. (b) An XRD pattern of yttria-doped $BaZrO_3$ powder synthesized by calcining a mixture of $BaCO_3$ and YSZ at 1250°C for 2 h.

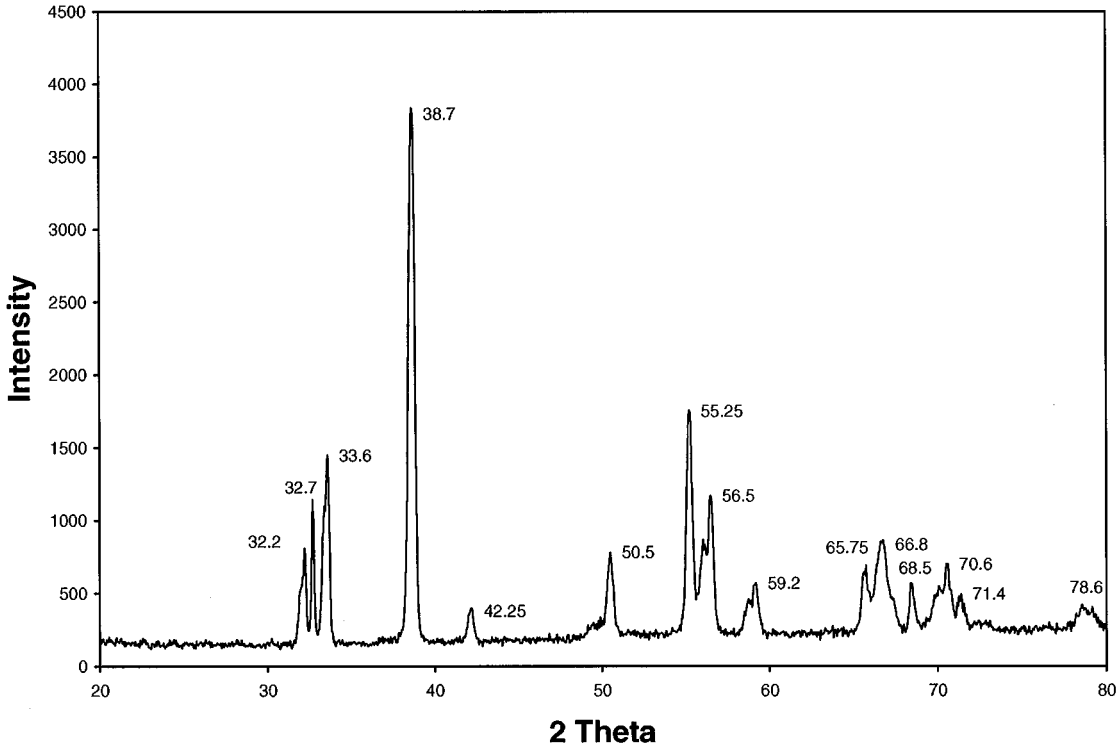

FIG. 2. XRD pattern of yttria-doped Na_2ZrO_3 powder synthesized by calcining a mixture of Na_2CO_3 and YSZ at 1250°C for 2 h.

For the yttria-doped Na_2ZrO_3 (Y–Na_2ZrO_3) precursor, since Na_2ZrO_3 readily reacts with water by a reaction such as

$$Y\text{–}Na_2ZrO_3 + 2H_2O \rightarrow 2NaOH + Y_2O_3\text{–}ZrO_2, \quad [2]$$

repeated boiling in deionized water, filtering, and washing was adequate to completely remove Na_2O as NaOH. In this case also, the chemical analysis showed that the solution contained predominantly Na, but only trace amounts of Y and Zr (Table 2). In order to determine the purity of the as-washed powders, chemical analysis was performed using the inductively coupled plasma (ICP) technique by dissolving YSZ powders synthesized using both precursors in concentrated HCl. Table 3 gives the results of this analysis. It is seen that for the case of YSZ made with Y–Na_2ZrO_3, the concentrations of Zr^{4+} and Y^{3+} in the solution are in accord with expected concentrations of Zr and Y in YSZ. However, in the case of YSZ made using Y–$BaZrO_3$, the concentration of Y^{3+} is lower than expected on the basis of the starting powder. This suggests that some of the yttrium was leached out in dilute HNO_3. In both cases, the concentrations of Na^+ and Ba^{+2} are in the ppm level, indicating that the concentrations of these impurities in the powders are small (on the order of $\sim$0.5 wt.% or less in the respective YSZ powders). Some of this may, in part, be related to the possible incomplete washing of the powders, and not necessarily an indication of impurities dissolved in the YSZ powders.

XRD patterns of leached and washed powders synthesized from the two precursors are given in Fig. 3a. In both cases, the XRD patterns of leached and washed

TABLE 2
Chemical Analysis of the Leaching Solution (Water) after Boiling Y–Na_2ZrO_3 in It

Powder	Sodium (mol/l)	Yttrium (mol/l)	Zirconium (mol/l)
Y–Na_2ZrO_3	0.713	$< 5 \times 10^{-5}$	$< 5 \times 10^{-5}$

TABLE 3
Chemical Analysis of the Synthesized YSZ Nanosize Powders

Sample	Zr^{4+} (wt.%)	Y^{3+} (wt.%)	Ba^{2+} (ppm)	Na^+ (ppm)
YSZ made using Y–Na_2ZrO_3	0.095	0.017	—	7
YSZ made using Y–$BaZrO_3$	0.21	0.01	12	—

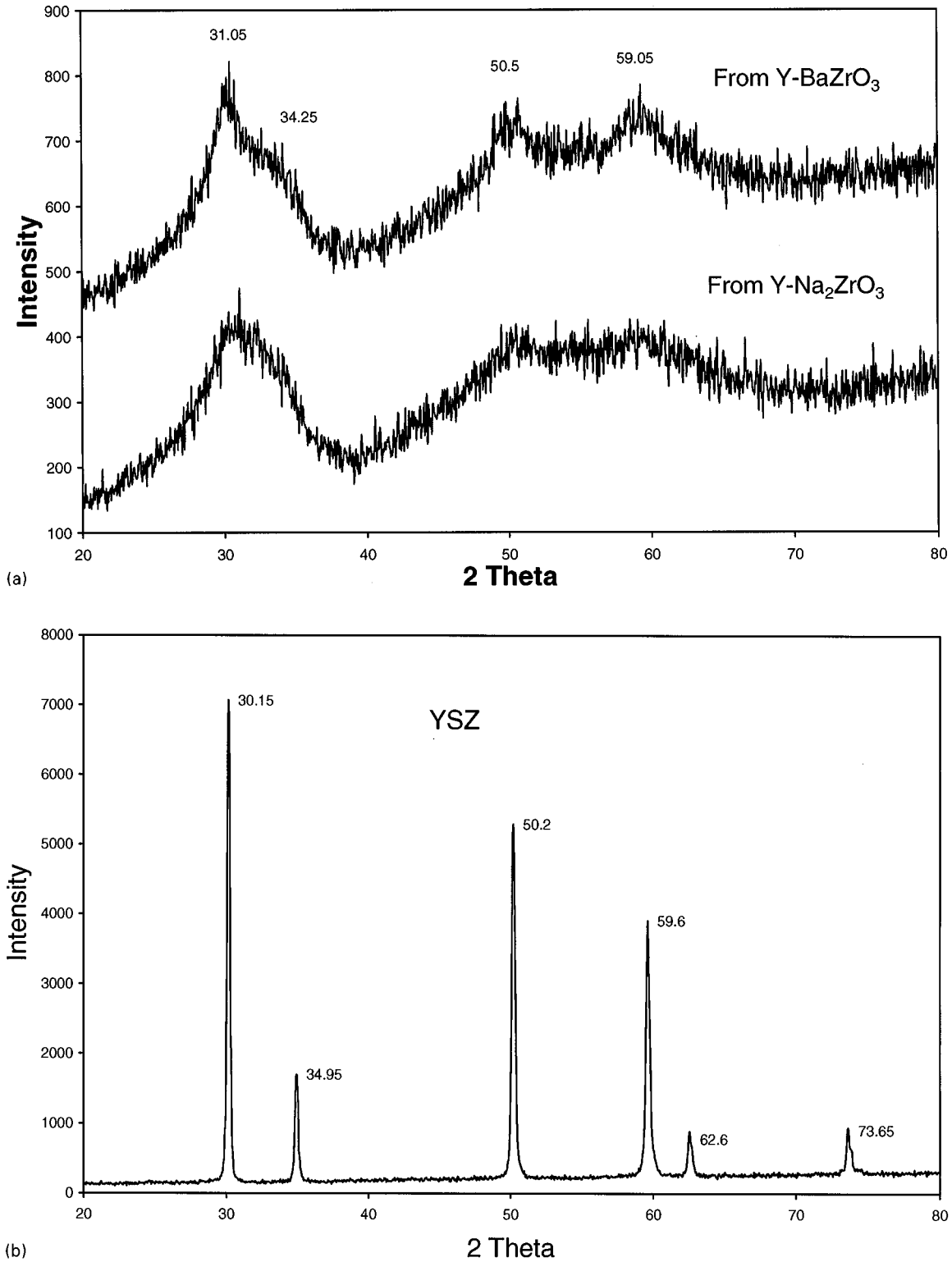

FIG. 3. (a) XRD patterns of the residue after boiling Y–$BaZrO_3$ in dilute HNO_3 (after leaching Ba) and washing in water, and of the residue after boiling Y–Na_2ZrO_3 in deionized water (after leaching Na) and washing in water. (b) XRD pattern of a commercial YSZ powder.

powders were quite different from those of the corresponding precursors (Y–Na_2ZrO_3 and Y–$BaZrO_3$). At the same time, the XRD patterns of the leached and washed powders were nearly identical, regardless of the precursor used, Y–Na_2 ZrO_3 or Y–$BaZrO_3$. Figure 3b shows an XRD pattern of commercial YSZ. It is readily seen that the XRD patterns of leached and washed powders are similar to those of the commercial YSZ, insofar as peak positions are concerned. This shows that during leaching of the respective precursors, only BaO or Na_2O is leached away, resulting in a residue containing Y, Zr, and O such that the Zr–Y–O skeleton has either a cubic or a tetragonal symmetry. The large peak broadening observed in XRD patterns makes it impossible to determine whether the phase formed is cubic or tetragonal, since there is only a small difference in the XRD patterns of the two phases. The XRD peaks in the patterns of leached powders are very broad, indicative of a very fine particle size. This shows that very fine (nanosize) particles of YSZ can be formed starting with precursors (Y–$BaZrO_3$ or Y–Na_2ZrO_3) whose particle size is several microns.

The formation of nanosize powders, starting with coarse precursor powders, can be illustrated via the following example. Let us consider the reaction of Y–$BaZrO_3$ with dilute HNO_3. The precursor, Y–$BaZrO_3$, is essentially insoluble in dilute HNO_3. However, it can react with HNO_3, as given by Eq. [1]. Although the following illustration assumes that the formed structure of YSZ is cubic, the general conclusions concerning the accompanying volume change, leading to the formation of nanosize powders, are independent of the structure formed. The volume of a Y–Ba ZrO_3 unit cell is about 73.72 $Å^3$. One unit cell of cubic zirconia contains four formula units, i.e., four "ZrO_2" or four "Y–ZrO_2," with a volume of $\sim$135.72 $Å^3$. Thus, per one formula unit, such as that created by one Y–$BaZrO_3$ unit cell, the volume is 135.72/4, or 33.93 $Å^3$. That is, as Y–$BaZrO_3$ reacts with HNO_3 to form Y–ZrO_2, there is a net change in volume from 73.72 $Å^3$ to 33.93 $Å^3$. This is equivalent to a $(73.72 - 33.93)/73.72 \times 100 \approx 54\%$ decrease in volume. In terms of a linear change, this corresponds to a $(\sqrt[3]{73.72} - \sqrt[3]{33.93})/\sqrt[3]{73.72} \times 100 \approx 25\%$ decrease in a linear dimension. As the surface of the precursor particle reacts with HNO_3 to form soluble $Ba(NO_3)_2$, there is a substantial volume change and a linear change (a decrease), which should lead to cracks and fissures at the unit cell (A) level. This should thus lead to the formation of tiny fragments at the angstrom or nanometer level. As the product, Y–ZrO_2, is insoluble (or has a very low solubility) in the liquid used, Ostwald ripening, which requires dissolution, transport, and reprecipitation, should not occur. Figure 4 shows a schematic of the leaching process of Y–$BaZrO_3$ in dilute HNO_3. The outer layer of the particle becomes porous since BaO (as $Ba(NO_3)_2$) is leached out of Y–$BaZrO_3$. Further reaction occurs by the transport of HNO_3 to the porous YSZ/dense Y–$BaZrO_3$ interface, reaction to form $Ba(NO_3)_2$ and YSZ, and the transport of dissolved $Ba(NO_3)_2$ away from the interface, through the porous YSZ, into the acid bath. The porous YSZ is easily fragmented into a very fine powder. Thus, even though the original Y–$BaZrO_3$ powder is coarse, the resulting YSZ powder should be nanosize. A similar mechanism is expected to be operative during the synthesis of nanosize YSZ starting with Y–Na_2ZrO_3. This is the origin of the molecular decomposition process for the synthesis of nanosize powders. The preceding also suggests that the initial precursor particle size should have no bearing on the final size of nanoparticles. Indeed, nanosize powder can be synthesized using precursors that are considerably coarse, for example several microns in size.

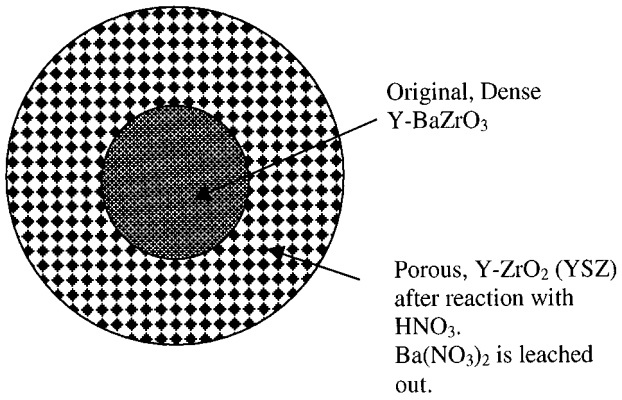

FIG. 4. Schematic showing a particle of Y–$BaZrO_3$ reacting with HNO_3. The porous outer layer is YSZ. The dense inner region is the original Y–$BaZrO_3$. The reaction involves the following steps: (i) transport of HNO_3 through the porous YSZ layer to the porous YSZ/dense Y–$BaZrO_3$ interface; (ii) reaction between Y–$BaZrO_3$ and HNO_3 to form soluble $Ba(NO_3)_2$ and insoluble, porous YSZ; (iii) transport of $Ba(NO_3)_2$ through the porous YSZ layer into the acid bath.

The Scherrer formula relates the average particle size, d, to X-ray peak broadening, B, by

$$d = \frac{0.9\lambda}{B \cos\theta} \qquad [3]$$

In order to determine the peak broadening attributable only to the particle size effect, a commercial YSZ powder was sintered at 1500°C for a few hours to obtain a strain-free, coarse-grained (grain size on the order of a few microns) sample. An XRD pattern of the sample was obtained. Peak width (at half the peak height) from this sample for a given (hkl), in the present case (111), was subtracted from the corresponding peak width of the leached and washed powders. In this manner, line broadening attributable to the instrument as well as the presence of both $K\alpha_1$ and $K\alpha_2$,

TABLE 4
Particle Size (nm) of As-Synthesized Nanosize YSZ Powder and the Powder after Being Heated in Air at Various Temperatures

Thermal treatment conditions	YSZ from $Y–BaZrO_3$, d in nm	Thermal treatment conditions	YSZ from $Y–Na_2ZrO_3$, d in nm
As washed	2.4	As-washed	2.4
350°C/1.5 h	8.0	300°C/1.5 h	4.8
450°C/1.5 h	10	350°C/1.5 h	17
650°C/1.5 h	23	650°C/1.5 h	18
1000°C/5 h	37	1000°C/5 h	31

could be corrected for. The corrected peak width was measured to be approximately 4° (~0.07 radians) for the case of the as-washed powders, which is equivalent to an average crystallite size of about a few nanometers (~2 to ~3 nm) for both of the as-washed powders (Table 4).

As an independent confirmation of the nanosize of the powders formed, specific surface area measurements were conducted using the BET adsorption isotherm method. The surface area measurements were made on both of the precursors ($Y–Na_2ZrO_3$ and $Y–BaZrO_3$) and the synthesized powders. The specific surface area of the precursors was typically only ~3 m^2/g (Table 5), consistent with the large particle size of the precursors. The specific surface area of the naonosize powder made from the Na_2ZrO_3 precursor, however, was measured to be around 67 m^2/g. Assuming particles to be spherical for simplcity, the diameter of the particle can be estimated from the relation

$$d = 6/S\rho, \qquad [4]$$

where ρ is the density of YSZ and S is the specific surface area. Assuming $\rho = 5.9\ g/cm^3$ for YSZ and 67 m^2/g for S (measured by BET), the diameter is estimated to be ~15 nm. Thus, specific surface area measurement also shows that the synthesized powder is indeed nanosize. However, the estimated particle size from surface area measurements is about 5 to 6 times greater than that estimated from XRD peak broadening. A possible reason for this may be the formation of agglomerates. In order to explore this possibility, samples were examined by transmission electron microscopy on a JEOL 4000FX TEM. For TEM examination, a sample of YSZ powder synthesized using $Y–BaZrO_3$ was suspended in alcohol and vibrated ultrasonically. Figure 5a shows a bright-field image of the sample at

TABLE 5
Surface Areas of As-Calcined Precursors, As-Synthesized Nanosize YSZ, and after the Nanosize YSZ after Being Heated to 1000°C for 5 h

Sample	$Y–BaZrO_3$	$Y–Na_2ZrO_3$	As-synthesized nanosize YSZ from $Y–Na_2ZrO_3$ precursor	Nanosize YSZ after 5 h at 1000°C
Surface area (m^2/g)	3.5	2.7	66.6	13.6

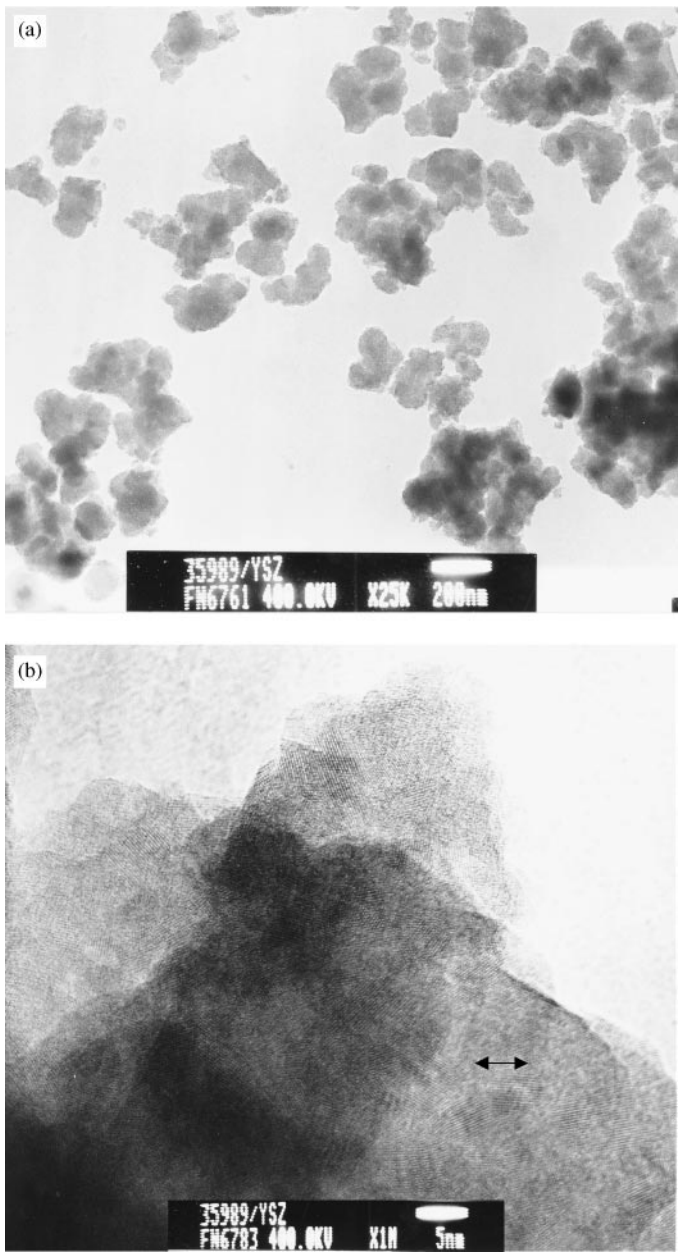

FIG. 5. (a) Bright-field TEM image of nanosize YSZ, synthesized using $Y–BaZrO_3$, at 25,000× showing agglomerates of ~50 to 200 nm in size. (b) Bright-field TEM image of the same sample at 1,000,000×, showing lattice fringes consistent with the formation of crystalline YSZ. The individual crystallite size is about 5 nm.

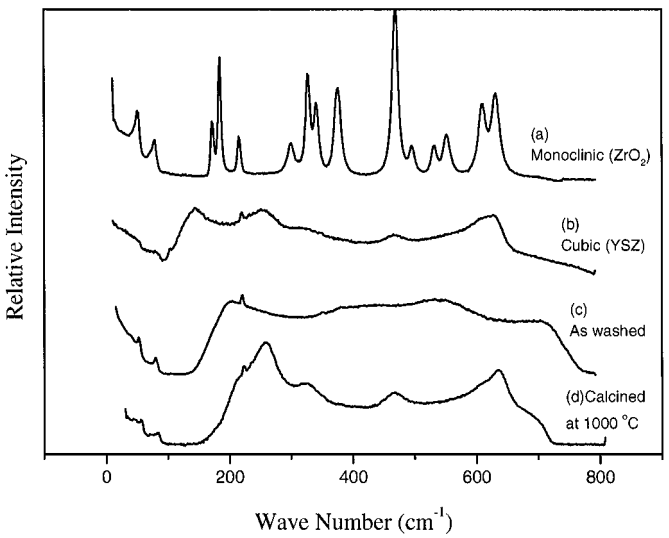

FIG. 6. Raman spectra of (a) monoclinic ZrO_2, (b) cubic YSZ, (c) as-washed YSZ powder (synthesized using Y–$BaZrO_3$), and (d) the same sample as in (c) after 5 h at 1000°C.

25,000×. It is seen that the observed particles, which are agglomerates, are in the range of 50 to 200 nm in size. A higher magnification image (1,000,000×) in Fig. 5b shows lattice fringes of individual particles in the agglomerates. As is evident from this micrograph, the individual crystallite size is about 5 nm, in reasonably good agreement with an estimate based on XRD peak broadening. The lattice image also shows that the as-synthesized powder is crystalline and not amorphous.

The above results conclusively demonstrate that nanosize YSZ powder can be effectively prepared by the molecular decomposition approach using alkali or alkaline earth metal oxide precursors. XRD patterns of the YSZ obtained from the two precursors are consistent with the formation of cubic zirconia. However, it is known that XRD peaks of cubic and tetragonal zirconia are very similar and thus difficult to delineate, especially when the peaks are rather broad. Thus, XRD is not a very good technique for distinguishing between cubic and tetragonal zirconia, especially if the crystallite size is in the nanometer range. However, Raman spectra of cubic, tetragonal, and monoclinic zirconia are quite different (28). For this reason, selected samples were examined by Raman spectroscopy, the results of which are discussed below.

Figures 6a and 6b are Raman spectra of monoclinic ZrO_2 and cubic (8 mol.% Y_2O_3-doped) zirconia obtained from commercial vendors, respectively. It is seen that the spectra of these two materials are quite different. The cubic structure of zirconia is characterized by a broad peak between 600 and 650 cm^{-1}, while the monoclinic spectrum contains several sharp lines. These results are similar to the ones reported in the literature (28). A spectrum of the tetragonal

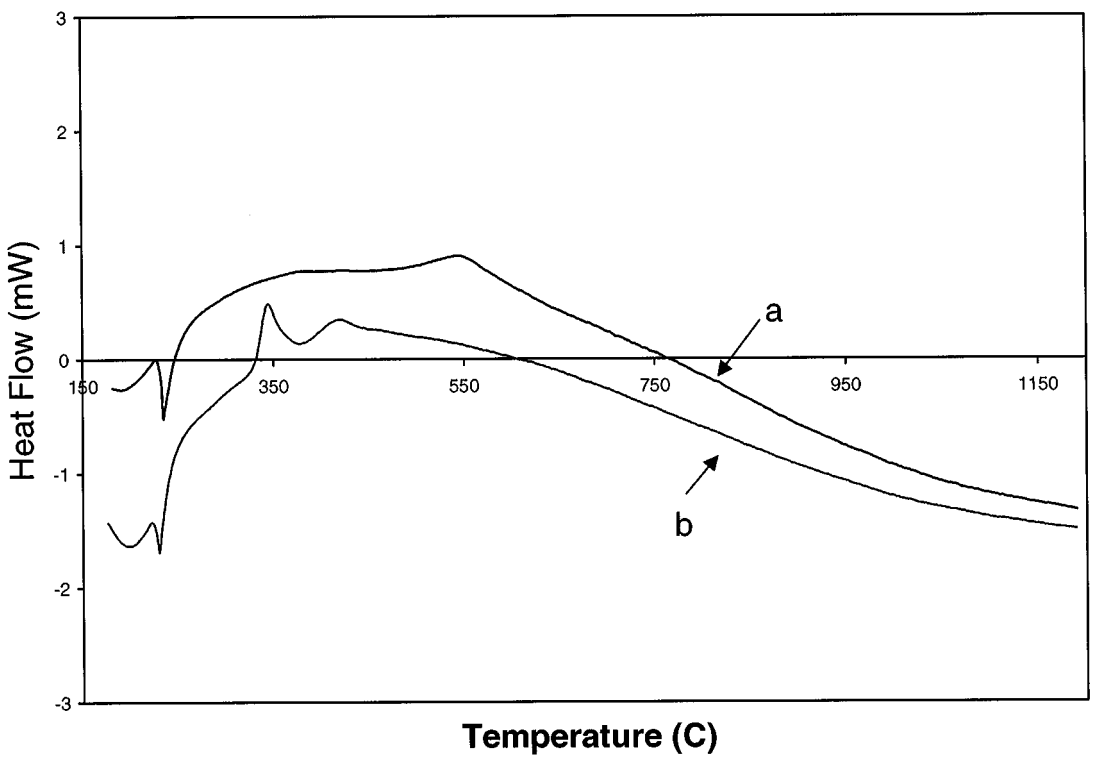

FIG. 7. DTA traces obtained at 10°C/min, in air, of nanosize YSZ powders synthesized from (a) Y–$BaZrO_3$ and (b) Y–Na_2ZrO_3 powders.

phase is known to exhibit characteristic lines at 260 cm^{-1}, 500 cm^{-1}, and 640 cm^{-1} (28). Figure 6c shows a spectrum of the as-synthesized nanosize powder made using Y–$BaZrO_3$. Note that this pattern is also characterized by the existence of rather broad peaks. The pattern shows no evidence of either the monoclinic or the tetragonal phases, and is similar to the cubic spectrum. Figure 6d is a spectrum of the synthesized powder after a thermal treatment at 1000°C for 5 h. This spectrum is also characterized by the presence of broad peaks. Peaks representative of a monoclinic phase are absent. However, the presence of humps at $\sim$260 cm^{-1} and $\sim$640 cm^{-1} may indicate the existence of a mixture of cubic and tetragonal phases. Note, however, that the same peaks are present in commercial YSZ as well.

In order to examine possible changes in the crystal structure of the synthesized nanosize YSZ powders, differential thermal analysis (DTA) on the as-washed powders was conducted. In addition, XRD patterns were obtained on powders after heat-treating the as-washed powders at various temperatures. Figure 7 shows the DTA traces of YSZ nanopowders synthesized from both precursors. The peaks centered at $\sim$235°C in the two traces are attributed to endothermic desorption of adsorbed water. The traces also show broad exothermic peaks in the temperature range from $\sim$300 to $\sim$600°C. An exothermic peak is usually attributed to the crystallization process, provided the as-formed powders are amorphous. In the present case, the as-synthesized powder is crystalline and not amorphous, as seen in the TEM micrograph given in Figure 6b, unlike some other YSZ powders prepared by sol–gel or chemical coprecipitation. In such cases, the exothermic peak due to the crystallization is generally well defined and sharp (21). In the present work, by contrast, the exothermic peak is very broad for powders made using either of the precursors, but more so in the case of nanosize YSZ powder made from Y–$BaZrO_3$ precursor, indicating that there is neither the occurrence of a distinct crystallization, nor the occurrence of a phase transition over the temperature range investigated. The broad exothermic peak may be attributed to the possible removal of point defects, and/or the occurrence of particle growth during the thermal treatment. The occurrence of particle growth during thermal treatment can be readily verified by XRD examination of nanosize YSZ powders heat-treated at various temperatures.

Figure 8 shows the XRD spectra of nanosize YSZ powders, synthesized from Y–$BaZrO_3$, thermally treated at various temperatures. It is seen that the crystal structure of the YSZ powder is essentially unaffected by the thermal treatment, all the way up to 1000°C, the maximum temperature to which the synthesized powders were heated. The structure of YSZ appears to be cubic, although the presence of a small amount of tetragonal phase cannot be ruled out.

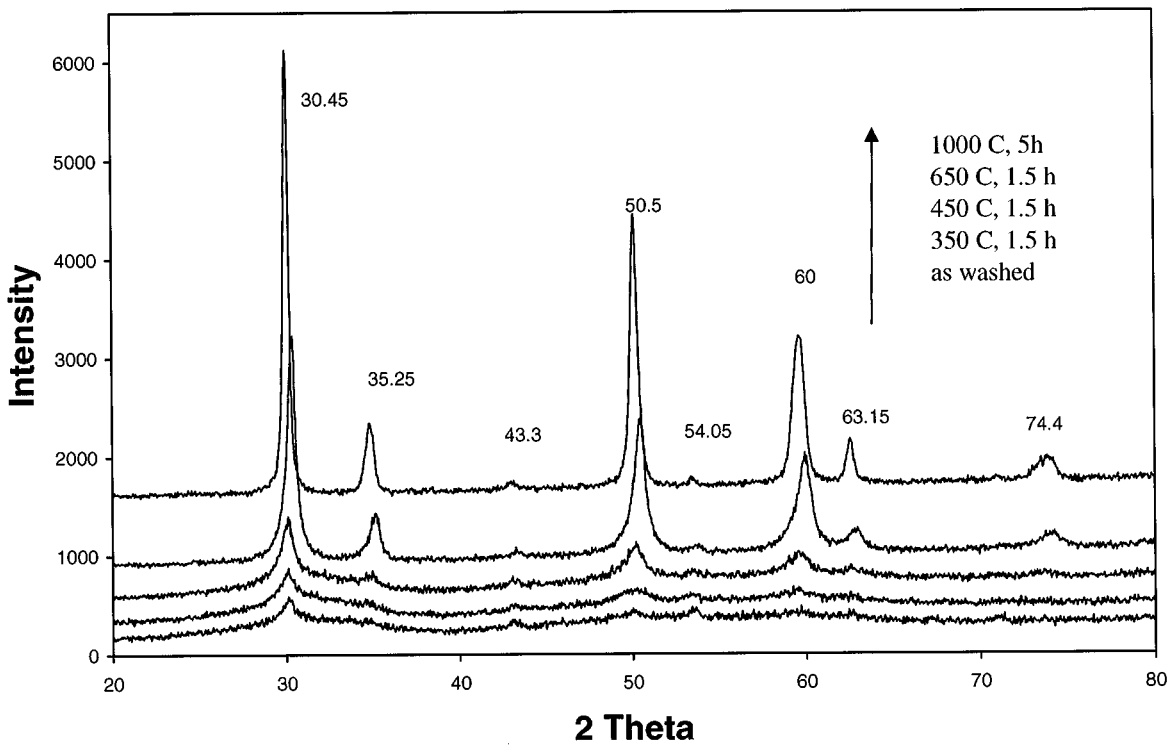

FIG. 8. XRD patterns of nanosize YSZ powders obtained from Y–$BaZrO_3$ subjected to subsequent thermal treatments at various temperatures.

The possible presence of a tetragonal phase will cause splitting of (200) and (220) peaks from the original peaks into (200)/(002) and (220)/(202) doublets. The approximate peak positions for these two sets of peaks (with Cu$K\alpha$ radiation) are $\sim 30.95^\circ$ and $\sim 50.27^\circ$, respectively. The XRD pattern of the powder after 5 h at 1000°C given in Fig. 8 shows that there is no evidence of peak splitting, indicating that even after 5 h at 1000°C, the powder remains cubic. Very small peaks observed in these patterns at $\sim 43.3^\circ$ and $\sim 54.05^\circ$ are due to the incomplete removal of the original precursor, Y–$BaZrO_3$. As the temperature of heat treatment is increased, the peak height increases at the expense of peak width, consistent with the occurrence of particle growth. The estimated particle size of the powders after heat treatment at 1000°C is about 37 nm, showing that the nanosize particles are relatively stable against significant growth at temperatures as high as 1000°C.

Nanosize YSZ obtained from the Y–Na_2ZrO_3 precursor was similarly subjected to various thermal treatments. The corresponding XRD patterns are given in Fig. 9, and the dependence of the particle size on the temperature of heat treatment is given in Table 4. It is seen that in this case also, even after heat treatment at 1000°C for 5 h, the average particle size is only about 31 nm. This shows that nanosize powder derived from Y–Na_2ZrO_3 is also stable against significant particle growth, up to 1000°C for 5 h. However, the XRD pattern of the powder heat-treated at 1000°C shows the presence of a small amount of monoclinic phase (characterized by two small peaks on either side of the (111) peak at $\sim 30.05^\circ$). It is not clear if this is the result of possible low-level sodium as an impurity. The other possibility is that in the original precursor formulation, not all of the Na_2ZrO_3 was doped with Y_2O_3. That is, there may have been some Na_2ZrO_3 present with little or no Y_2O_3 dissolved in it. The presence of some undoped Na_2ZrO_3 cannot be ruled out on the basis of XRD results. If some undoped Na_2ZrO_3 is present, it is expected to form nanosize, undoped ZrO_2 upon boiling in water. The as-synthesized, undoped zirconia is expected to be cubic rather than monoclinic by virtue of the lower surface energy of the cubic phase compared to the monoclinic phase. When heated to a high temperature where growth of particles occurs, the monoclinic phase will become the stable phase. The formation of some monoclinic phase when heated to 1000°C, as evidenced in Fig. 9, may be related to the possible existence of some undoped Na_2ZrO_3 in the precursors. Table 4 gives the average particle size of YSZ powders, treated at various temperatures after synthesis, calculated from the Scherrer formula using the half peak widths from the XRD patterns given in Figs. 8 and 9. The particle sizes of YSZ from both precursors are similar, in the range from a few nanometers to tens of nanometers after thermal treatment at

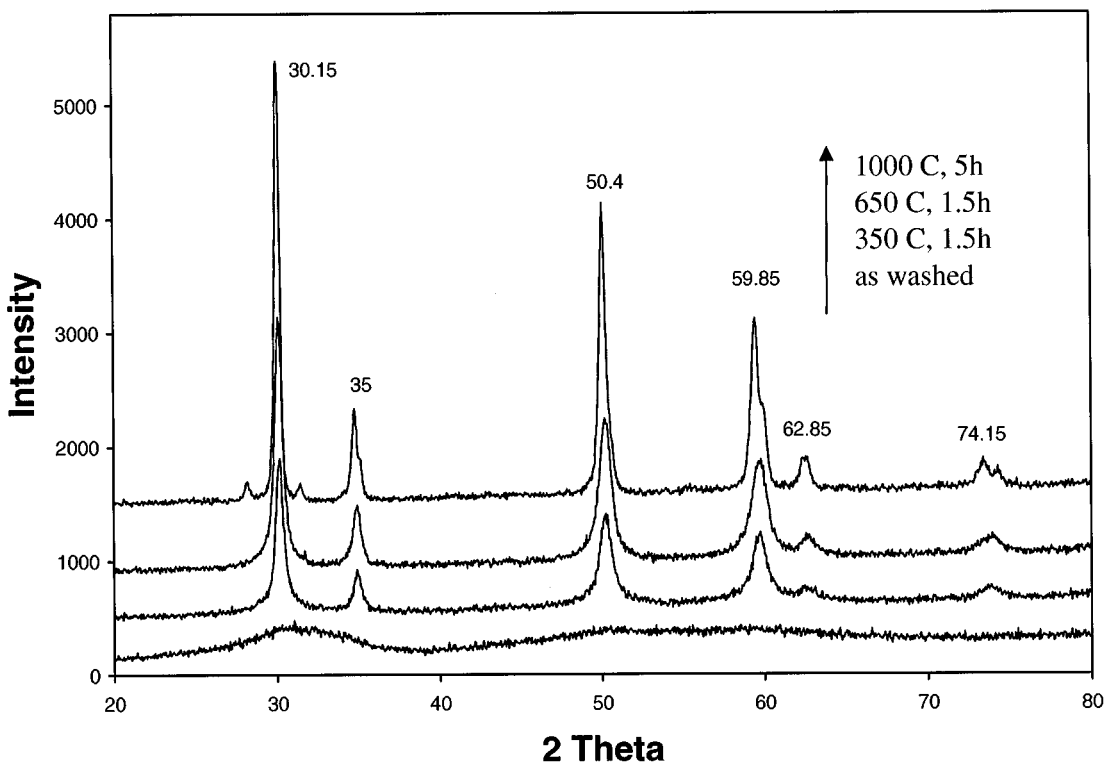

FIG. 9. XRD patterns of nanosize YSZ powders obtained from Y–Na_2ZrO_3 subjected to subsequent thermal treatments at various temperatures.

a temperature as high as 1000°C. An investigation of the sinterability of YSZ powders made by the present process, and the measurement of ionic conductivity of sintered samples, is underway. The results of these studies will be reported in a separate communication.

IV. CONCLUSIONS

Nanosize yttria-stabilized zirconia (YSZ) powder was prepared by a novel approach, in which yttria-doped $BaZrO_3$ or yttria-doped Na_2ZrO_3 precursors were first synthesized by a solid-state reaction. The unwanted species, BaO or Na_2O, was then leached away by washing the precursors in a dilute HNO_3 solution or in water. This led to the formation of very fine, nanosize YSZ. The particle size of the as-synthesized YSZ powders was a few nanometers and increased to tens of nanometers after thermal treatment at a temperature as high as 1000°C.

ACKNOWLEDGMENTS

This work was supported by the U.S. Department of energy, NETL, contract No. DE-AC26-99FT40713.

REFERENCES

1. J. Y. Ying, *in* "Nanophase Materials: Synthesis—Properties—Applications" (G. C. Hadjipanayis and R. W. Seigel, Eds.), NATO ASI Series E: Applied Sciences, Vol. 260, pp. 37–44. Kluwer Academic Publishers, Dordrecht, 1994.
2. G. Skandan, *NanoStructured Mater.* **5**(2), 111–126 (1995).
3. L. V. Interrante and M. J. Hampden-Smith, "Chemistry of Advanced Materials: An Overview." Wiley-VCH, New York, 1998.
4. M. L. Trudeau and J. Y. Ying, *NanoStructured Mater.* **7**(1–2), 245–258 (1996).
5. Y. X. Li, O. Koper, M. Atteya, and K. J. Klabunde, *Chem. Mater.* **4,** 323–330 (1992).
6. T. Boronia, K. J. Klabunde, and G. B. Sergeev, *Environ. Sci. Technol.* **29,** 1511–1517 (1995).
7. N. Herron, *Chem. Technol.* **19,** 542–548 (1989).
8. H. J. Fecht, *in* "NANOMATERIALS: Synthesis, Properties and Applications" (A. S. Edelstein and R. C. Cammarata, Eds.), pp. 89–110. Institute of Physics Publishing, Bristol and Philidelphia, 1996.
9. K. J. Klabunde, J. V. Stark, O. Koper, C. Mohs, A. Khaleel, G. Glavee, D. Zhang, C. M. Sorensen, and G. Hadjipanayis, *in* Ref. (1), pp. 1–19.
10. C. M. Sorensen, Q. Li, H. K. Xu, Z. X. Tang, K. J. Klabunde, and G. C. Hadjipanayis, *in* Ref. (1), pp. 109–116.
11. H. Gleiter, *in* "Deformation of Polycrystals: Mechanism and Microstructures" (N. Hansen, A. Horsewell, T. Leffers, and H. Lilholt, Eds.), p. 15. Riso National Laboratory, Rackilde, Denmark, 1981.
12. D. D. Beck and R. W. Seigel, *J. Mater. Res.* **7,** 2840–2845 (1992).
13. H. W. Sarkas, S. T. Arnold, J. H. Hendricks, L. H. Kidder, C. A. Jones, and H. K. Bowen, *Z. Phys. D* **26,** 46–50 (1993).
14. A. S. Tschope and J. Y. Ying, *NanoStructured Mater.* **4,** 617 (1994).
15. A. Rouanet, G. Pichelin, C. Roucau, E. Snoeck, and C. Monty, *in* Ref. (1), pp. 85–88.
16. Z. X. Tang, S. Nafis, C. M. Sorensen, G. C. Hadjipanayis, and K. J. Klabunde, *IEEE Trans. Mag.* **25,** 4236–4238 (1989).
17. Z. X. Tang, S. Nafis, C. M. Sorensen, G. C. Hadjipanayis, and K. J. Klabunde, *J. Magn. Mater.* **80,** 285–289 (1989).
18. T. Benameur, R. Yavari, and R. Durand, *Mater. Sci. Eng. A* **181/182,** 1145–1149 (1994).
19. M. L. Trudeau, J. Y. Huot, R. Schultz, D. Dussault, A. Van Neste, and G. L'Espe'rance, *Phys. Rev. B* **45,** 4626–4636 (1992).
20. D. E. Brown, M. N. Mahmood, A. K. Turner, S. M. Hall, and P. O. Fogarty, *Int. J. Hydrogen Energy* **7,** 405 (1982).
21. T. Okubo and H. Nagamoto, *J. Mater. Sci.* **30,** 749–757 (1995).
22. P. Mondal and H. Hahn, *Ber. Bunsen-Ges.* **101**(11), 1765–1768 (1997).
23. J. Grabis, A. Ruzjukevics, D. Rasmane, M. Mogensen, and S. Linderoth, *J. Mater. Sci.* **33**(3), 723–728 (1998).
24. T. L. Wen, V. Herbert, S. Vilminot, and J. C. Bernier, *J. Mater. Sci.* **26,** 5184–5188 (1991).
25. J. Joseph, *J. Aerosol Sci.* **29**(5/6), 721–736 (1998).
26. A. V. Virkar and S. V. Bhide, A Molecular Decomposition Process for the Synthesis of Naonosize Powders, patent application filed December 1998.
27. I. Barin, "Thermochemical Data of Pure Substances," 3rd ed. VCH, Weinheim, New York, 1995.
28. C. G. Kontoyannis and M. Orkoula, *J. Mater. Sci.* **29,** 5316–5320 (1994).